Available online at www.sciencedirect.com
ScienceDirect
Journal of Nuclear Materials 367–370 (2007) 440–445
journal of nuclear materials
www.elsevier.com/locate/jnucmat

Microstructure of helium-implanted and proton-irradiated T91 ferritic/martensitic steel

Z. Jiao *, N. Ham, G.S. Was

University of Michigan, Department of Nuclear Engineering and Radiological Sciences, Ann Arbor, MI 48109, United States

Abstract

In the effort to understand the effect of helium on the irradiated microstructure, the ferritic/martensitic steel T91 was implanted to three helium concentrations of 720 appm, 1260 appm and 1800 appm. The alloy with and without helium pre-implantation was irradiated with 2.0 MeV protons to doses of 2.2 dpa, 7 dpa and 9.2 dpa at 450 °C. The irradiated microstructure, consisting of dislocation loops and bubbles, was characterized using transmission electron microscopy (TEM). Small bubbles were found in helium pre-implanted samples. No cavities were observed in irradiated samples without helium pre-implantation. Helium was found to promote swelling in T91. Irradiation may not be sufficient for cavity nucleation. However, when combined with helium pre-implantation, irradiation plays a role by assisting bubble growth and promoting swelling.

1. Introduction

Ferritic/martensitic alloys are proposed as candidate structural materials for fusion reactors, Generation IV reactors, and accelerator-driven spallation neutron transmutation systems (ADS). Understanding radiation effects in these alloys is critical for their success in advanced reactor and transmutation systems. An excellent summary of the status of knowledge of ferritic/martensitic steels for application in fusion and spallation systems can be found in reference [1].

One primary concern about the F/M steels' application in a fusion or spallation environment is swelling. Experiments [2–5] have shown that F/M steels are highly resistant to swelling, with swelling rates that are much lower than those in austenitic steels. A potential aggravating factor is the production of He due to transmutation reactions. Experiments described in [6–9] have been conducted to simulate the effect of helium production in fusion and spallation systems on swelling and microstructural evolution by doping with He producing elements or via helium pre-implantation. Maziasz, et al. [6] found that when 2% Ni was added to HT9, the incubation dose for void formation decreased from ~150 dpa to ~50 dpa. Although it is becoming clear that helium may have significant effects on the performance of this alloy for spallation applications, the full extent of this effect is not fully understood.

The objective of this research is to study the effect of helium pre-implantation and proton irradiation

* Corresponding author. Fax: +1 734 7634540.
E-mail address: zjiao@umich.edu (Z. Jiao).

0022-3115/$ - see front matter © 2007 Elsevier B.V. All rights reserved.
doi:10.1016/j.jnucmat.2007.03.118

on the microstructure of T91. Proton irradiation has already proven to be effective at emulating neutron damage in austenitic stainless steels [10]. When combined with helium pre-implantation, proton irradiation is expected to be an excellent technique to study helium effects in T91.

2. Experimental

The composition of T91 used in this study is Fe–8.37Cr–0.9Mo–0.21Ni–0.45Mn–0.22V–0.28Si–0.1C. The as-received T91 was normalized at 1066 °C for 46 min and then tempered at 790 °C for 42 min. The result of the processing is a ferritic/martensitic microstructure with a grain size of ~10 μm. The carbides are preferentially located on grain boundaries. Samples with a dimension of 2 mm × 1.5 mm × 20 mm were fabricated from the bulk T91 alloy. Prior to helium implantation, the sample surface was first ground to a final finish using #4000 SiC grit paper, then electropolished in a 10% perchloric acid in methanol solution at −30 °C. The helium implantation was done in the Tandetron Accelerator at the Michigan Ion Beam Laboratory. Three helium concentrations of 720 appm, 1260 appm and 1800 appm were achieved using 3.0 MeV He++ with the sample at room temperature. Implantations were done using a custom-designed energy degradation wheel to evenly distribute the He over the range 1–4 μm. The samples with and without helium pre-implantation were then irradiated to three doses of 2.2 dpa, 7 dpa and 9.2 dpa using 2.0 MeV protons at 450 °C. The dose rate was 2×10^{-5} dpa/s. During irradiation, the sample temperatures were monitored using a Stinger thermal imager and the sample temperatures were kept well within 450 ± 10 °C. The helium concentrations and irradiation doses were specially selected to meet a He/dpa ratio of ~180 appm/dpa. This concentration ratio is expected in an ADS environment.

Specimens for transmission electron microscopy (TEM) were made from the irradiated samples by first grinding off the excess material from the unirradiated side. Then 3 mm disks were cut using an ultrasonic slurry cutter. The disks were mechanically thinned to less than 100 μm to reduce the amount of magnetic material and then jet-thinned until perforation in a 2% perchloric acid, 15% butyl cellusolve and 83% methanol solution at −40 °C. The microstructure of the irradiated T91 was characterized using a JOEL 2010F analytical transmission electron microscopy at the Michigan Electron Microbeam Analysis Laboratory at University of Michigan.

3. Results

3.1. Helium pre-implantation microstructure

Unirradiated T91 has a martensite lath structure as shown in Fig. 1(a). Carbide precipitates were found at grain boundaries and lath and subgrain boundaries. A tangled dislocation network and dislocation cells were also found in the unirradiated T91. After helium implantation, the line dislocation

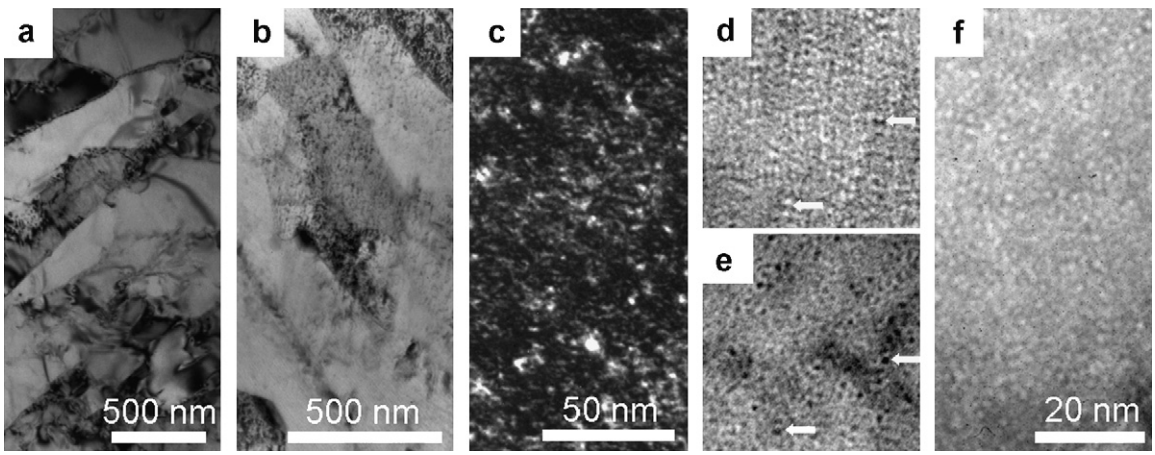

Fig. 1. TEM photographs of microstructures in unirradiated and helium pre-implanted T91 (a) unirradiated, bright field, (b) 1260 appm He, bright field, (c) 1260 appm He, weak beam dark field with $B = 001$, $g = 020$, (d) and (e) underfocus and overfocus bubble image in T91 with 720 appm He and (f) bubbles in 1260 appm He T91.

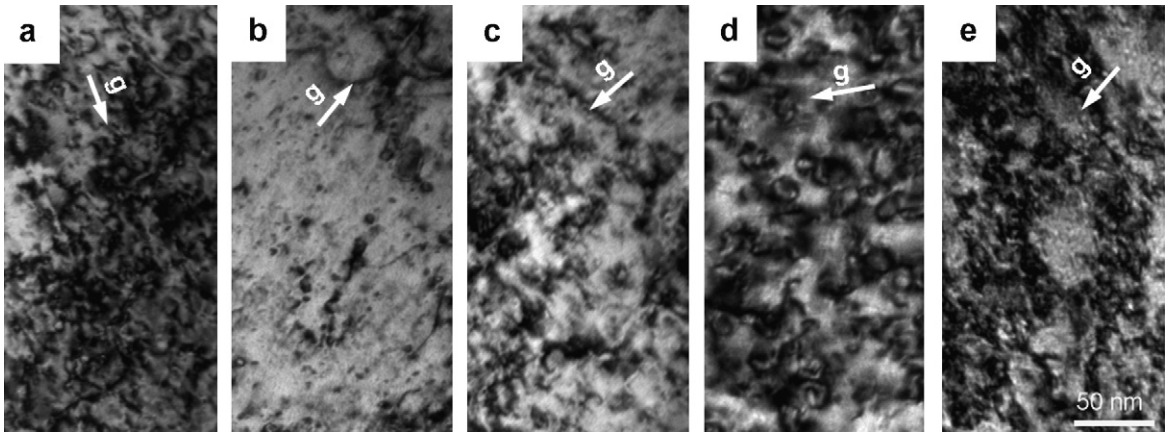

Fig. 2. Bright field TEM photographs of irradiation microstructure in T91 at various doses and helium concentrations (a) 0 appm He: 2.2 dpa, (b) 720 appm He: 2.2 dpa, (c) 1260 appm He: 2.2 dpa, (d) 0 appm He: 7 dpa and (e) 1800 appm He: 7.0 dpa. Photographs were taken near [1 1 1] zone axis with $g = 1\,-1\,0$.

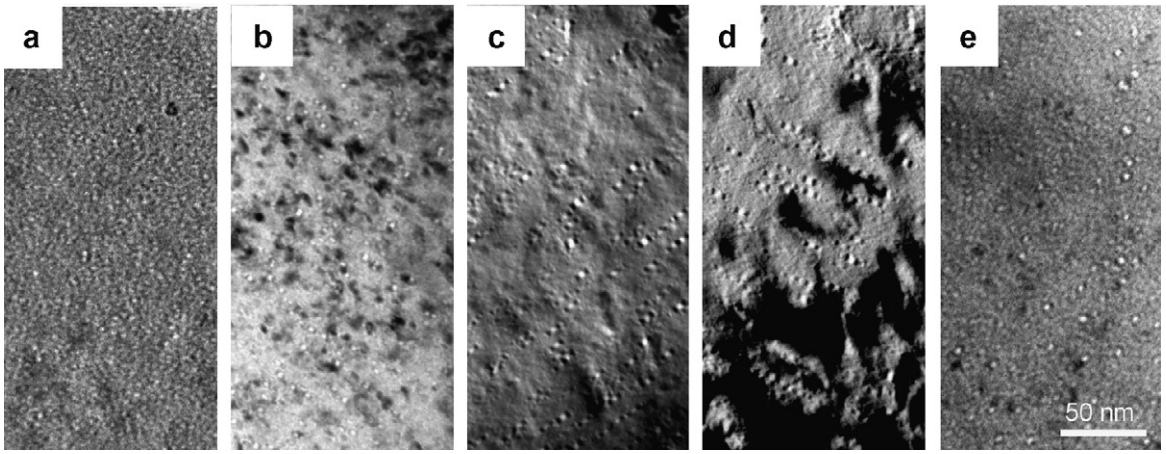

Fig. 3. Bright field TEM photographs of bubbles in T91 at various doses and helium concentrations (a) 720 appm He: 2.2 dpa, (b) 720 appm He: 7 dpa, (c) 1260 appm He: 7 dpa, (d) 1800 appm He: 7 dpa and (e) 1260 appm He: 9 dpa.

density decreases while the irradiation-induced defect density increases (Fig. 1(b)). A weak beam dark field TEM image (Fig. 1(c)) shows a high density of small defect clusters and dislocation loops (~3 nm in diameter) in the helium pre-implanted T91. Helium bubbles were observed at all three helium concentrations. Fig. 1(d) shows a bubble image taken in an underfocus condition in a 720 appm He sample with defocus $\Delta f = -500$ Å and (Fig. 1(e)) shows a bubble image in an overfocus condition with $\Delta f = +500$ Å in the same area. As indicated by the arrows, bubbles change from bright to black dots, which is a characteristic image of small bubbles under and over focus. Bubble size slightly increases as the helium concentration increases (Fig. 1(f)) and the average bubble size is 1.0 nm in 720 appm He samples and 1.2 nm and 1.4 nm in 1260 appm and 1800 appm He samples, respectively. The bubble density was found to be on the order of 10^{23} m^{-3}. The swelling increases with helium concentration. It is <0.01% in 720 appm He samples and ~0.02% in 1800 appm He samples.

3.2. Proton irradiation microstructure

Fig. 2 shows the microstructure evolution of T91 irradiated to various doses at 450 °C with and without helium pre-implantation. Figs. 2(a) and (d) show the microstructure of T91 irradiated to 2.2 dpa and 7 dpa, respectively, without helium pre-implantation. Dislocation loops are a major

feature for these conditions. Figs. 2(b) and (c) show the microstructure of T91 irradiated to 2.2 dpa with 720 appm and 1260 appm helium concentration, respectively. A low density of line dislocations was observed in these samples. As the irradiation dose increases, the dislocation loop density increases (Fig. 2(e)).

Fig. 3 shows the bubble structure in T91 irradiated to various doses at 450 °C with different helium concentrations. Figs. 3(a) and (b) show the effect of irradiation dose on bubble growth in 720 appm He samples. As the dose increases from 2.2 dpa to 7 dpa, the bubble size increases from 1.3 nm to 1.9 nm. Figs. 3(b), (c) and (d) show the helium concentration effect on bubble structure in samples irradiated to 7 dpa. As seen in these three figures, the bubble size in 720 appm He samples is smaller than that in samples with higher helium concentration. Fig. 3(e) shows the bubble structure in 1260 appm He samples irradiated to 9 dpa at 450 °C. Compared to those irradiated to 7 dpa with the same level of helium concentration (*c*), no significant difference in bubble structure was observed.

4. Discussion

4.1. State of helium in bubbles

The state of helium contained in the bubbles at the end of the implantation and subsequent irradiation can be evaluated by comparing the average number of the helium atoms (n_a) in a bubble to the maximum number of helium atoms allowed (n_{max}) in the bubble under thermodynamic equilibrium conditions. If the ratio of n_a/n_{max} is greater than one, the bubbles are overpressurized. If the ratio is less than one, the bubbles are in a more stable state. Assuming all the helium atoms are in the bubbles after implantation, n_a can be calculated by dividing the total number of implanted helium atoms by the total number of bubbles. The maximum number of helium atoms allowed in a bubble can be estimated using the equation of the state of dense gas: $n_{max} = PV/ZKT$, where P is the maximum helium pressure allowed in the bubble, V is the bubble volume, Z is the compressibility factor and K is the gas constant. Under thermodynamic equilibrium, $P = 2\gamma/r$, where γ is the surface energy and r is the bubble radius.

The calculated n_a/n_{max} ratios for various helium implantation and irradiation conditions are listed in Table 1. The ratios for the samples without proton-irradiation (first data column) are all greater than one, which means that the bubbles after the helium implantation are overpressurized. The formation of overpressurized bubbles is probably due to the lack of thermal vacancies as the implantations were performed at room temperature. The subsequent proton-irradiations produce a large number of vacancies, some of which are absorbed by the overpressurized bubbles resulting in a lower pressure and more stable bubbles ($n_a/n_{max} < 1$). The helium pressure inside the bubbles decreases dramatically at a dose of only 2.2 dpa. Higher irradiation doses further decrease the helium pressure, but less significantly.

Table 1
Calculated n_a/n_{max} ratios

	0 dpa	2.2 dpa	7 dpa	9.2 dpa
720 appm	1.2	0.6	0.4	0.3
1260 appm	1.4	0.6	0.5	0.4
1800 appm	1.3	0.7	0.7	0.6

4.2. Effect of helium on microstructure

Prior to proton irradiation, T91 samples with He pre-implantation have high density of small bubbles and interstitial clusters. This is consistent with the literature [11], in which T91 was implanted with 23 MeV α particles to a He concentration of 5000 appm at 550 °C and voids and black dot interstitial clusters were discovered in the samples. However, in that study, voids were found to form on prior austenite grain boundaries, lath and subgrain boundaries, at dislocations inside the lath structure and at carbide-matrix interfaces. In the present study, bubbles were found to nucleate uniformly throughout the sample and no preferential sites were observed. The likely reason for this discrepancy is that our helium implantation was done at room temperature instead of high temperature (550 °C), so that helium could not diffuse over long distances in the matrix. In an earlier study of the same alloy at the same temperature, no bubbles were formed in samples with a helium concentration of 100 appm [12]. Also at this low dose, the data in the literature indicates that several hundred ppm He is required for bubbles to form.

Fig. 4 shows the effect of helium concentration on dislocation loops, bubbles and swelling in irradiated T91. As shown in Figs. 4(a) and (b), with increasing helium concentration, dislocation loop

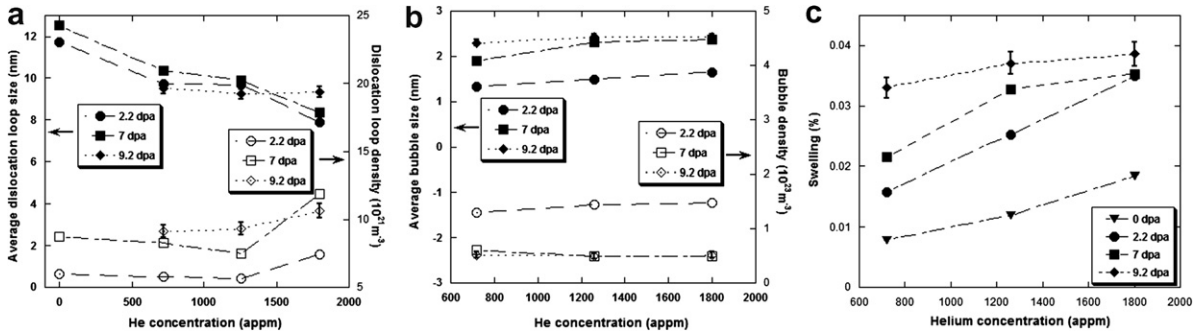

Fig. 4. Helium effect on (a) average dislocation loop size and density, (b) average bubble size and density and (c) swelling in T91 irradiated at 450 °C.

size decreases while bubble size increases. Dislocation loops appear to be larger in the sample without pre-implanted He. It is likely that the He bubbles act as defect sinks and impede the growth of dislocation loops. Bubble density does not show a strong dependence on helium concentration and loop density is insensitive to He concentration except at the highest level. As shown in Fig. 4(c), helium promotes swelling in T91. Stronger dependence of swelling on helium concentration was found in lower dose samples. The mechanism by which helium promotes swelling is yet to be understood.

4.3. Effect of irradiation dose on microstructure

Fig. 5 shows the effect of irradiation dose on dislocation loops, bubbles and swelling in irradiated T91. Loop size is relatively independent of dose but loop density increases with increasing dose. Irradiation has little effect on loop size but higher density is expected in higher dose samples. The bubble size increases while the number density decreases with dose for all He levels and they appear to approach saturation by 9.2 dpa. However, much higher dose may be needed to examine bubble growth behavior.

Swelling shows a strong dependence on irradiation dose (Fig. 5(c)) in helium pre-implanted T91. The swelling in the 720 appm He sample tripled when it was irradiated to 9.2 dpa. Although the overall swelling rate is smaller in the 1800 appm He samples, the swelling still doubles over the course of less than 10 dpa. It is noteworthy that irradiation alone may not be sufficient for cavity nucleation as no cavities were identified in T91 irradiated to 10 dpa [12]. However, once bubbles are nucleated with the help of helium implantation, irradiation will play a much more important role by assisting bubble growth and promoting swelling.

5. Summary

Prior to proton-irradiation, bubbles were observed in helium-implanted T91. The average bubble size was found to be 1.0 nm in 720 appm He samples and 1.4 nm in 1800 appm He samples.

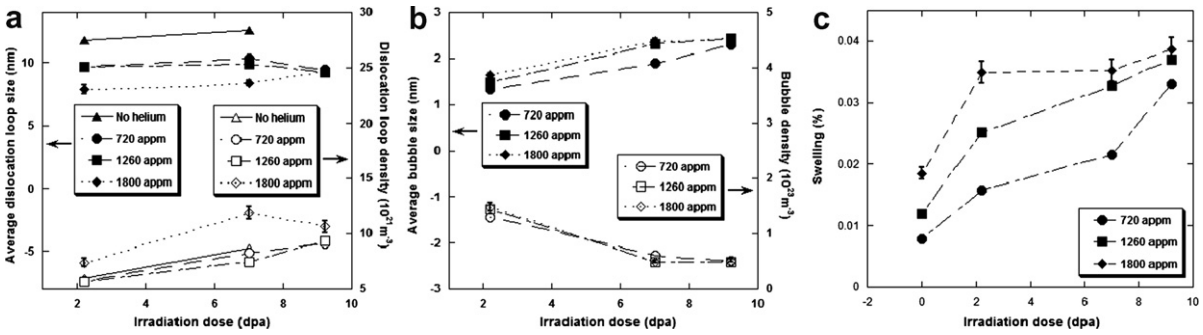

Fig. 5. Irradiation dose effect on (a) average dislocation loop size and density (b) average bubble size and density and (c) swelling in T91 irradiated at 450 °C.

The bubble density was found to be on the order of $10^{23}\,m^{-3}$. The swelling slightly increases with increasing helium concentration from <0.01% at 720 appm He to ~0.02% at 1800 appm.

No cavities were observed in irradiated samples without helium pre-implantation. The average bubble size slightly increases while density decreases with helium concentration. The pre-implanted helium promotes swelling in T91. The average dislocation loop size is the largest in samples without helium and it slightly decreases as the helium concentration increases. He bubbles induced by helium-implantation may act as defect sinks and impede the growth of dislocation loops.

No significant effect of irradiation on dislocation loop size was observed regardless of helium concentration, but the loop density increases by about a factor of 2 between 2.2 dpa and 9.2 dpa. Irradiation alone may not be sufficient for void nucleation. However, irradiation does affect bubble growth and promote swelling when combined with helium pre-implantation.

Acknowledgement

The authors gratefully acknowledge Victor Rotberg and Ovidiu Toadar for their assistance in conducting proton irradiations. The authors also acknowledge the facilities provided by the Michigan Ion Beam Laboratory and the Electron Microbeam Analysis Laboratory at University of Michigan. Support for this research was provided by the Department of Energy under contract #73713-001-03 8T.

References

[1] R.L. Klueh, Proceedings of the Symposium on Materials for Spallation Neutron Sources, The Minerals, Metals, & Materials Society, 1997, p. 67.
[2] D.S. Gelles, J. Nucl. Mater. 233–237 (1996) 293.
[3] M.B. Toloczko, F.A. Garner, J. Nucl. Mater. 233–237 (1996) 289.
[4] J.J. Kai, R.L. Klueh, J. Nucl. Mater. 230 (1996) 116.
[5] N. Hashimoto, R.L. Klueh, J. Nucl. Mater. 305 (2002) 153.
[6] P.J. Maziasz, R.L. Klueh, J.M. Vitek, J. Nucl. Mater. 141–143 (1986) 929.
[7] E. Wakai, N. Hashimoto, Y. Miwa, J.P. Robertson, R.L. Klueh, K. Shiba, S. Jistukawa, J. Nucl. Mater. 283–287 (2000) 799.
[8] E. Wakai, K. Kikuchi, S. Yamamoto, T. Aruga, M. Ando, H. Tanigawa, T. Taguchi, T. Sawai, K. Oka, S. Ohnuki, J. Nucl. Mater. 318 (2003) 267.
[9] E. Wakai, T. Sawai, K. Furuya, A. Naito, T. Aruga, K. Kikuchi, S. Yamashita, S. Ohnuki, S. Yamamoto, H. Naramoto, S. Jistukawa, J. Nucl. Mater. 307–311 (2003) 278.
[10] G.S. Was, J.T. Busby, T. Allen, E.A. Kenik, A. Jensson, S.M. Bruemmer, J. Gan, A.D. Edwards, P.M. Scott, P.L. Andreson, J. Nucl. Mater. 300 (2002) 198.
[11] J. Henry, M.-H. Mathon, P. Jung, J. Nucl. Mater. 318 (2003) 249.
[12] G.S. Was, J.T. Busby, T.R. Allen, J. Gan, Proceedings of the Sixth International Meeting on Nuclear Applications of Accelerator Technology (AccApp '03), 864–873, American Nuclear Society, La Grange Park, IL (2004).